Available online at www.sciencedirect.com
ScienceDirect
Journal of Solid State Chemistry 181 (2008) 920–934
JOURNAL OF SOLID STATE CHEMISTRY
www.elsevier.com/locate/jssc

Crystal structure of the new compound $Pb_{3+x}Sb_{3-x}S_{7-x}Cl_{1+x}$ ($x\sim0.45$): The homologous series $Pb_{(2+2N)}(Sb,Pb)_{(2+2N)}S_{(2+2N)}(S,Cl)_{(4+2N)}Cl_N$ and its polychalcogenide derivatives ($N = 1$–3)

Charlotte Doussier, Yves Moëlo*, Alain Meerschaut, Philippe Léone, Catherine Guillot-Deudon

Institut des Matériaux Jean Rouxel (IMN), Université de Nantes, CNRS, 2 rue de la Houssinière, BP 32229, 44322 Nantes Cedex 3, France

Received 6 November 2007; received in revised form 24 January 2008; accepted 27 January 2008
Available online 9 February 2008

Abstract

The new chloro-sulfosalt $Pb_{3+x}Sb_{3-x}S_{7-x}Cl_{1+x}$ ($x\sim0.45$) has been synthesized at 500 °C from a mixture of PbS, $PbCl_2$ and Sb_2S_3. It crystallizes in the orthorhombic system (space group *Pbam*), with $a = 15.194(3)$ Å, $b = 23.035(5)$ Å, $c = 4.0591(8)$ Å, $V = 1420.6$ Å^3, $Z = 4$. The crystal structure has been solved by X-ray single-crystal study, with a final $R = 0.0497$. Deviation from stoichiometric $Pb_3Sb_3S_7Cl$ (x coefficient) follows the substitution rule $Sb^{3+} + S^{2-} \rightarrow Pb^{2+} + Cl^-$. Sb and Pb sub-positions within mixed (Sb,Pb) sites are discussed; Pb excess precludes any superstructure along c. A unique pure Cl position is bound only to Pb atoms with a distorted square coordination. The title compound is a rod-type structure derived from the SnS archetype, homeotypic with $Pb_6Sb_6S_{14}(S_3)$, where the $(S_3)^{2-}$ trimer is replaced by two Cl^-; this substitution is quite isovolumic. Other similar structures are: three polychalcogenides $Sr_6Sb_6S_{14}(S_3)$, $Pb_6Sb_6Se_{14}(Se_3)$ and $Eu_6Sb_6S_{14}(S_3)$; $KLa_{1.28}Bi_{3.72}S_8$ and its Ln isotypes; dadsonite, $Pb_{23}Sb_{25}S_{60}Cl$. $Pb_{3+x}Sb_{3-x}S_{7-x}Cl_{1+x}$ is the $N = 2$ member of the homologous series $Pb_{(2+2N)}(Sb,Pb)_{(2+2N)}S_{(2+2N)}(S,Cl)_{(4+2N)}Cl_N$; the $N = 1$ member corresponds to the previously known $\sim Pb_{4.3}Sb_{3.7}S_{8.7}Cl_{2.3}$ compound. Other polychalcogenide derivatives of this homologous series are $K_2Pr_{2-x}Sb_{4+x}Se_8(Se_4)$ and its Ln isotypes ($N = 1$), as well as $SrBiSe_3$ ($N = 3$). Such a comparative modular analysis allowed to propose a structural model for the previous synthetic "Phase Y", $\sim Pb_{10}Sb_{10}S_{23}Cl_4$, corresponding to the combined $N = (1 + 2)$ homolog.

Keywords: Lead; Antimony; Chloro-sulfide; Crystal structure; Homologous series; Polychalcogenide

1. Introduction

According to crystal structure databases, there are less than 100 of complex compounds of the chloro-chalcogenide type $(M1,M2,\ldots)_xQ_yCl_z$ (Q = S, Se, Te), associating chlorine and a chalcogen Q with two cations M or more. Among them, the sub-group of chloro-chalcogenosalts, where at least one cation is a pnictogen, principally Sb or Bi, is the best represented, as illustrated by recent studies dealing with various transition metals (Mn, Fe, Cu, Ag, Cd, Hg, Nb) as second cation: Mn ($MnSbS_2Cl$ [1]; $MnBiS_2Cl$ [2]), Fe ($FeSbS_2Cl$ [3]), Cu and Ag ($Cu_3Bi_2S_4Cl$ [4]; $Cu_{6.2}PS_5Cl$ [5]; $CuBiSCl_2$ and $AgBiSCl_2$ [6]; $AgBi_2S_2Cl_3$ [7]; $Ag_2Bi_2S_3Cl_2$ [8]; $AgBi_2S_3Cl$ and $AgBi_2Se_3Cl$ [9]; $Ag_{1.2}Bi_{17.6}S_{23}Cl_8$ and $Ag_{3x}Bi_{5-3x}S_{8-6x}Cl_{6x-1}$ [10]), Cd ($CdSbS_2Cl$ and $CdBiS_2Cl$ [11]), Hg (Hg_3AsS_4Cl and Hg_3AsSe_4Cl [12]), Nb ($NbP_4Se_3Cl_5$ and $Nb_2P_4S_4Cl_{10}$ [13]). Non-transition-metal compounds deal with Al ($AlSb_2Te_2Cl_4$ [14]; $Al_4Bi_4(S/Se)_4Cl_{16}$ [15]; $Al_4Bi_4Te_4Cl_{16}$ [16]), In ($InBi_2S_4Cl$ [17]) and Pb.

According to published data, Pb is combined quite exclusively with Sb to form lead–antimony chloro-sulfosalts, except for the mineral vurroite, $Pb_{20}Sn_2(Bi,As)_{22}S_{54}Cl_6$ [18,19]. Pb–Sb chloro-sulfosalts constitute a complex family, which has been essentially described up to now in the field of mineralogical studies, as natural compounds or synthetic derivatives. Table 1 lists these minerals and related synthetics. Including the results of this study, 18 compounds (9 minerals and 9 synthetics) have been

*Corresponding author.
E-mail address: yves.moelo@cnrs-imn.fr (Y. Moëlo).

0022-4596/$ - see front matter © 2008 Elsevier Inc. All rights reserved.
doi:10.1016/j.jssc.2008.01.041

Table 1
Natural and synthetic lead–antimony chlorosulfosalts and related compounds

Compound	Formula	Pb/(Pb + Sb)	Cl/(Cl + S)	*Me*/*An*	Note	References
Dadsonite	$Pb_{23}Sb_{25}S_{60}Cl$	0.479	0.016	0.787	STR	[20,21]
Pellouxite	$(Cu,Ag)_2Pb_{21}Sb_{23}S_{55}ClO$	0.447	0.018	0.768	STR	[22]
Playfairite	$\sim Pb_{16}(Sb,As)_{19}S_{44}Cl$	0.457	0.022	0.778	UC	[23,24]
Pillaite	$Pb_9Sb_{10}S_{23}ClO_{0.5}$	0.474	0.042	0.792	STR	[25]
Mineral C	$\sim Pb_{17}Sb_{18}S_{43}Cl_2$	0.486	0.044	0.778	UC	[26]
Mineral C1	$\sim AgPb_8Sb_8S_{20}Cl$	0.500	0.048	0.762	Chem.	[26]
Phase V	$\sim Pb_2Sb_2S_{4.76}Cl_{0.31}$	0.500	0.061	0.800	XRPD	[27]
Synthet. K95	$Pb_{12.65}Sb_{11.35}S_{28.35}Cl_{2.65}$	0.527	0.086	0.774	STR	[28]
Phase Y	$\sim Pb_{11}Sb_{10}S_{23}Cl_4$	0.521	0.143	0.778	STRM	[20], this study
Mn-OClS	$\sim Mn_{0.7}Pb_{11.0}Sb_{11.3}S_{25.3}Cl_{4.7}O$	0.493	0.157	0.742	STR	[29]
Phase Y'	$\sim Pb_{19}Sb_{18}S_{42}Cl_8$	0.514	0.160	0.740	UC	[20], this study
Ardaite	$\sim Pb_{19}Sb_{13}S_{35}Cl_7$	0.594	0.167	0.762	UC	[30]
Phase B	$\sim Pb_7Sb_8S_{16}Cl_{3.4}$	0.467	0.175	0.773	XRPD	[27]
Synthet.	$Pb_{4+x}Sb_{4-x}S_{9-x}Cl_{2+x}$	0.575	0.181	0.750	STR	This study
Ardaite (?)	$\sim Pb_{10}Sb_6S_{17}Cl_4$	0.625	0.191	0.762	Chem.	[31]
Phase A	$\sim Pb_9Sb_8S_{19}Cl_{4.5}$	0.529	0.192	0.723	UC	[27]
Synthet. K97	$Pb_{4+x}Sb_{4-x}S_{9+x}Cl_{2+x}$	0.540	0.211	0.727	STR	[32]
Unnamed mineral	$\sim Pb_2SbS_3Cl$	0.667	0.250	0.750	Chem.	[33]

Me/*An*: cation/anion atomic ratio; STR: full structural characterisation; STRM: structure model; UC: unit cell determined; XRPD: X-ray powder diagram, without unit cell characterisation; and Chem.: chemical analysis only.
Classification according to an increasing Cl/S atomic ratio.

described, but they are often poorly characterized. These compounds frequently present large unit cells (up to ~10,000 Å^3), combined with a complex chemical formula, like for the mineral pellouxite $(Cu,Ag)_2Pb_{21}Sb_{23}S_{55}ClO$ [22]. This formula, as well as those of dadsonite, $Pb_{23}Sb_{25}S_{60}Cl$ [20,21], and pillaite, $Pb_9Sb_{10}S_{23}ClO_{0.5}$ [25], points to an original feature, that is the ability of chlorine to give specific compounds, even with a very low Cl/S atomic ratio.

The present study deals first with a new synthetic lead–antimony chloro-sulfide, $Pb_{3+x}Sb_{3-x}S_{7-x}Cl_{1+x}$, which appears structurally very close to the polysulfosalt $Pb_6Sb_6S_{14}(S_3)$ [34]. Owing to comparative modular analysis, it has led to a general re-examination of the crystal chemistry of related lead–antimony chloro-sulfosalts. This has permitted to define a new homologous series, with parent polychalcogenides, and to propose a structure model for another synthetic chloro-sulfosalt.

2. Experimental

2.1. Synthesis of $Pb_{3+x}Sb_{3-x}S_{7-x}Cl_{1+x}$

$Pb_{3+x}Sb_{3-x}S_{7+x}Cl_{1+x}$ was synthesized by solid-state reaction of stoichiometric amounts of PbS, $PbCl_2$ and Sb_2S_3 (5:1:3). The starting materials were homogenized by grinding, put into a sealed evacuated silica tube and heated at 500 °C for 10 days. Some individual needles could be extracted from the massive powder. The sample and its purity were characterized by X-ray powder diffraction (Siemens D5000, Cu$K\alpha_1$, $\lambda = 1.54051$ Å). Some powder was included in epoxy and prepared as a polished section to permit its examination with polarized reflected-light microscopy, as well as with scanning electron microscope equipped with energy dispersive spectrometer (SEM-EDS). On the basis of a total of 6 cations, SEM-EDS analysis gave the formula $Pb_{3.4(1)}Sb_{2.6(1)}S_{6.4(2)}Cl_{1.3(1)}$, close to the result of the crystal structure study.

2.2. Crystal structure determination of $Pb_{3+x}Sb_{3-x}S_{7-x}Cl_{1+x}$

Several crystals of $Pb_{3+x}Sb_{3-x}S_{7+x}Cl_{1+x}$ were selected for X-ray single-crystal study, using a Nonius Kappa CCD diffractometer with Mo$K\alpha$ radiation ($\lambda = 0.71073$ Å). For the best crystal, fixed on the top of a glass capillary, reflection intensities were collected with an exposure time of 120 s/plate, φ varying from 0° to 360° with an increment of 1°. The crystal-to-detector distance was set to 36 mm ($\theta_{max} = 35°$), and the images were processed with a program package [35,36].

The crystal structure was solved in the space group *Pbam* (no. 55) using direct methods (SHELXTL program [37]) for heavy atoms, and Fourier difference series for the other ones. All atoms except mixed (Sb,Pb) sites were refined with anisotropic displacement parameters. Absorption correction (indexed face option) was applied using the Gaussian method.

The crystal structure of the final non-stoichiometric formula, $Pb_{3+x}Sb_{3-x}S_{7-x}Cl_{1+x}$, is presented in Fig. 1. To obtain it, in a first step, pure non-split Pb, Sb, S and Cl positions with full occupancy were fixed, giving the stoichiometric formula $Pb_3Sb_3S_7Cl$. The unique pure Cl position was distinguished from the seven S positions according to its coordination as well as bond valence calculations (see below). While the three pure Pb positions were clearly localized, without any significant electron residue or abnormal U value, the three Sb independent

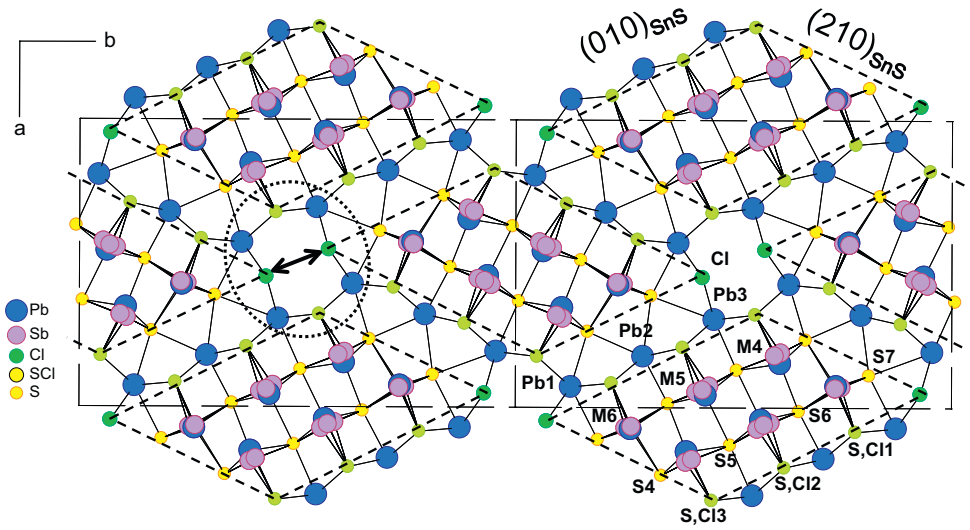

Fig. 1. Projection along c of the crystal structure of $Pb_{3+x}Sb_{3-x}S_{7+x}Cl_{1+x}$. The rod-based architecture is outlined (dashed lozenges). See Fig. 3 for comparison with the SnS structure. The ellipse (doted-line) points the connection between four rods, and the double arrow between two acute edges along b.

positions appeared as mean positions ($M4$–$M6$), which ought to be split into Sb and Pb sub-positions. In a first step, for every three M sites, a first split has discriminated two positions, one on the m mirror ($z = 0$), the second one with a small shift along z. They were attributed to pure Sb atoms. After this second step, the three highest electron residues were localized near these split Sb positions; they were attributed for each one to a Pb position (according to longer M–S distances—see below). A final electron residue, localized within the central $M5$ site, was attributed to a third Sb position on the mirror.

Relative to the stoichiometric formula $Pb_3Sb_3S_7Cl$, some Pb substituting for Sb in M sites must be counterbalanced by an equivalent substitution of Cl for a neighboring S atom, according to the heterovalent substitution rule: $Sb^{3+} + S^{2-} \rightarrow Pb^{2+} + Cl^{-}$ [26]. As S ($Z = 17$) and Cl ($Z = 18$) have quite identical X-ray scattering factors, it was not possible here to precise the partitioning of this Cl excess among S positions, neither on the basis of the diffraction data, nor through bond valence calculations. Nevertheless, due to the affinity of Cl towards Pb relatively to Sb in chloro-chalcogenides (see for instance the structure of $Pb_9Sb_{10}S_{23}ClO_{0.5}$ [25]), the Cl excess was located on S1–S3 positions, with a s.o.f. equal to the s.o.f. of the Pb position in the adjacent M site. With such a partitioning, when one (S,Cl) site is occupied by a Cl atom, this Cl atom will be bound exclusively to Pb atoms.

The final refinement converged to a reliability factor $R = 0.0497$, corresponding to the final formula $Pb_{3.45}Sb_{2.55}S_{6.55}Cl_{1.45}$, or $Pb_{3+x}Sb_{3-x}S_{7-x}Cl_{1+x}$ with $x \sim 0.45(3)$ for the selected crystal. The doubling of this formula approaches the stoichiometric one $Pb_7Sb_5S_{13}Cl_3$. The crystallographic data and the results of the structure refinement are compiled in Table 2. The atomic coordinates are given in Table 3, and the list of anisotropic displacement parameters in Table 4.

Table 2
Crystallographic data for the X-ray structure determination of $Pb_{3+x}Sb_{3-x}S_{7+x}Cl_{1+x}$

Compound	$Pb_{3.45}Sb_{2.55}S_{6.55}Cl_{1.45}$
Formula weight ($g\,mol^{-1}$)	1286.66
Crystal system	Orthorhombic
Space group	*Pbam* (no. 55)
Crystal size (mm^3)	$0.02 \times 0.02 \times 0.53$
Color/shape	Black/needle
A (Å)	15.194(3)
B (Å)	23.035(5)
c (Å)	4.0591(8)
V ($Å^3$)	1420.6(5)
Z	4
D_{calc} ($g\,cm^{-3}$)	6.016
μ (mm^{-1})	46.712
T (K)	293(2)
θ_{max} (deg)	35.00
$h\,k\,l$ value	$-21 \leqslant h \leqslant 21$
	$-29 \leqslant k \leqslant 32$
	$-5 \leqslant l \leqslant 5$
No. reflections; R_{int}	2332; 0.0731
No. independent reflections (obs; all)	1651
No. refined parameters	98
R_1 ($I \geqslant 2\sigma(I)$; all)	0.0497; 0.0812
wR_2 ($I \geqslant \geqslant 2\sigma(I)$; all)	0.1068; 0.1182
GoodF	1.087
Residual electronic density, e $Å^{-3}$	4.991 and −2.677

$R = \sum[|F_o| - |F_c|]/\sum[|F_o|]$; $R_w = [\sum w(|F_o| - |F_c|^2)/\sum wF_o^2]^{1/2}$ with $w = 1/\sigma(F_o)$.

3. Description of the crystal structure of $Pb_{3+x}Sb_{3-x}S_{7+x}Cl_{1+x}$

3.1. Atom coordination

According to Fig. 1, the three independent Pb positions have a triangular prismatic coordination; Pb1 and Pb3

Table 3
Atomic parameters (e.s.d.s.) and $U_{eq/iso}$ (in Å^2) for $Pb_{3+x}Sb_{3-x}S_{7+x}Cl_{1+x}$ at room temperature

Atoms		s.o.f.	x	y	z	$U_{eq/iso}$
Pb1	4*h*	1	0.4283(1)	0.3731(1)	0.5	0.0245(2)*
Pb2	4*g*	1	0.3222(1)	0.2074(1)	0	0.0222(2)*
Pb3	4*g*	1	0.1936(1)	0.0444(1)	0	0.0236(2)*
Sb4	8*i*	0.425(1)	0.3194(2)	−0.0946(1)	0.0582(6)	0.0231(6)
Sb4A	4*g*	0.10(1)	0.309(1)	−0.1086(8)	0	–
Pb4	4*g*	0.05(1)	0.346(2)	−0.107(1)	0	0.044(5)
Sb5	8*i*	0.30(1)	0.4390(3)	0.0704(3)	0.0532(8)	0.0137(8)
Sb5A	4*g*	0.10(1)	0.425(1)	0.0554(8)	0	–
Sb5B	4*g*	0.20(1)	0.4463(5)	0.0852(5)	0	–
Pb5	4*g*	0.10(1)	0.4568(7)	0.0636(5)	0	0.018(2)
Sb6	4*g*	0.40(2)	0.5710(3)	0.2474(3)	0	0.017(1)
Sb6B	8*i*	0.15(2)	0.5664(5)	0.2337(4)	0.091(3)	0.017(1)
Pb6	4*g*	0.30(1)	0.5746(4)	0.2356(3)	0	0.023(1)*
Cl	4*g*	1	0.5478(3)	0.4284(2)	0	0.0266(9)*
S1	4*g*	0.70(1)	0.4153(3)	0.2796(2)	0	0.0163(7)*
Cl1	4*g*	0.30(1)	–	–	0	–
S2	4*g*	0.90(1)	0.2911(3)	0.1167(2)	0	0.0169(7)*
Cl2	4*g*	0.10(1)	–	–	0	–
S3	4*g*	0.95(1)	0.1768(2)	−0.0494(2)	0	0.0155(7)*
Cl3	4*g*	0.05(1)	–	–	0	–
S4	4*h*	1	0.2362(3)	0.3349(2)	0.5	0.0251(9)*
S5	4*h*	1	0.3697(3)	−0.0074(2)	0.5	0.029(1)*
S6	4*h*	1	0.4871(3)	0.1498(2)	0.5	0.0256(9)*
S7	4*h*	1	0.6121(3)	0.3106(2)	0.5	0.028(1)*

* U_{iso}

Table 4
Anisotropic displacement parameters U^{ij} (in Å^2) for $Pb_{3+x}Sb_{3-x}S_{7+x}Cl_{1+x}$

Atom	U^{11}	U^{22}	U^{33}	U^{12}
Pb1	0.0304(4)	0.0250(4)	0.0182(3)	−0.0039(3)
Pb2	0.0231(3)	0.0256(4)	0.0179(3)	0.0013(4)
Pb3	0.0205(3)	0.0317(4)	0.0186(3)	−0.0043(3)
Cl	0.015(2)	0.040(3)	0.025(2)	−0.010(2)
(S,Cl)1	0.014(2)	0.020(2)	0.015(2)	−0.001(2)
(S,Cl)2	0.017(2)	0.020(2)	0.014(2)	−0.001(2)
(S,Cl)3	0.014(2)	0.020(2)	0.013(2)	−0.001(2)
S4	0.017(2)	0.023(2)	0.035(3)	−0.002(2)
S5	0.021(2)	0.036(3)	0.030(3)	0.007(2)
S6	0.015(2)	0.034(3)	0.027(2)	0.006(2)
S7	0.016(2)	0.028(2)	0.041(3)	0.006(2)

$U^{13} = U^{23} = 0$.

prisms are "standing" (= prism axis sub-perpendicular to the projection plane) bicapped (6 S atoms + 2 Cl atoms), while Pb2 prism is "lying" (= prism axis sub-parallel to the projection plane) monocapped, bound only to 7 S atoms. Bond valence sums calculated for these three Pb atoms according to Brese and O'Keeffe [38] are in a good agreement with the expected value +2 (Table 5).

The Cl atom is bound to lead atoms only (Fig. 2), with a quite regular square planar coordination, and a bond valence sum equal to 1.02 (Table 5), in quite accordance with a pure Cl filling. Such a coordination is very close to that of the pure Cl atom position bound to four Pb atoms at 3.007 Å in $Pb_{12.65}Sb_{11.35}S_{28.35}Cl_{2.65}$ [28], at 3.005 Å in $Pb_{4.32}Sb_{3.68}S_{8.68}Cl_{2.32}$ [32], at 2.972 (×2) and 3.0024 Å (×2) in $Pb_{23}Sb_{25}S_{60}Cl$ ("S1" position of Makovicky et al. [21]), or to four Bi atoms at 3.125 Å in $InBi_2S_4Cl$ [17].

The three (S,Cl) atoms have a square pyramidal coordination, more or less distorted according to the nature of the *M* cation. Considering short bonds, the coordinations of S5 and S6 are similar to the previous ones, but there are two additional long bonds (with 2 *M*5 and 2 *M*4, respectively). The quinary coordination of S7 corresponds to a triangular bipyramid, that of S4 to a "lying" trigonal prism.

The ligands of the three *M* polyhedra are constituted by one (S,Cl) and six S atoms. These six S atoms form a "standing" trigonal prism, capped by the (S,Cl) atom. Sb sub-positions are close to the capped face of the prism, while Pb positions are shifted towards the prism center. The bond valence calculations for these cations will be discussed below (see Section 4.2).

3.2. Rod-like organization of the crystal structure

According to Fig. 1, the crystal structure of $Pb_{3+x}Sb_{3-x}S_{7-x}Cl_{1+x}$ is built up from a single type of 1D block, a $M_{12}X_{16}$ rod (*M*: cation; *X*: anion) with lozenge section. According to the comparative modular analysis of lead sulfosalt structures [39,40], this rod is directly derived from the SnS archetype [41], by cutting along *c* a prism limited by (010) and (210) planes (Fig. 3). Relatively to the layered organization of SnS, this prism is two-layer (= four-atom) thick, and three hemi-octahedra large. Rods alternate along [110] and [$\bar{1}$10] according to two orientations, so that a $(010)_{SnS}$ face of a rod is in front of a $(210)_{SnS}$ face of an adjacent one.

3.3. Homeotypy with other chalcogenide structures

This crystal structure is homeotypic with four polychalcogenides, $Pb_6Sb_6S_{14}(S_3)$ (Fig. 4) [24,34], $Sr_6Sb_6S_{14}(S_3)$ [42], $Pb_6Sb_6Se_{14}(Se_3)$ [43], and $Eu_6Sb_6S_{14}(S_3)$ [44], as exemplified by the comparison of unit cell data (Table 6). Fig. 2 compares the environment of the Cl atom pair with that of the S_3 trimer in the polysulfide $Pb_6Sb_6S_{14}(S_3)$:

- the Cl–Cl distance is 3.604 Å, against 3.513 Å for the S5–S5 distance in the Pb polysulfide (corresponding distances in other S_3 groups: 3.499 Å in $Sr_6Sb_6S_{14}(S_3)$; 3.495 Å in $Eu_6Sb_6S_{14}(S_3)$; 3.359 Å in $Cs_5Sb_8S_{18}(HCO_3)$ [45]);
- the Cl–Pb distance is 3.007 (×2) and 3.069 (×2) Å, against 3.054, 3.113 (× 2) and 3.195 Å for the S5–Pb distance in the polysulfide.

Thus, $Pb_{3+x}Sb_{3-x}S_{7-x}Cl_{1+x}$ appears as a chemical derivative of $Pb_6Sb_6S_{14}(S_3)$ through the original heterovalent substitution $(S_3)^{2-} \rightarrow 2\,Cl^-$. The change in the unit cell volume is very weak ($\delta V/V \sim -5$‰—Table 6).

Table 5
Bond valence sums (BVS) for Pb and Cl pure positions in $Pb_{3+x}Sb_{3-x}S_{7+x}Cl_{1+x}$

Atom	(S,Cl)1 (s.o.f.: 0.7/0.3)	(S,Cl)2 (0.9/0.1)	(S,Cl)3 (0.95/0.05)	S4	S5	S6	S7	Cl	BVS
Pb1	2.965 × 2 /S: 0.23 × 2 /Cl: 0.09 × 2		3.140 × 2 /S: 0.19 × 2 /Cl: 0.01 × 2	3.048 0.26			3.142 0.20	3.007 × 2 0.28 × 2	2.06
Pb2	2.981 × 2 /S: 0.22 × 2 /Cl: 0.02 × 2	2.950 × 2 /S: 0.31 × 2 /Cl: 0.03 × 2		3.214 0.17		2.835 0.46	3.218 0.16		2.08
Pb3		3.105 × 2 /S: 0.20 × 2 /Cl: 0.02 × 2	2.975 × 2 /S: 0.30 × 2 /Cl: 0.02 × 2		2.930 0.36		3.561 0.07	3.069 × 2 0.23 × 2	1.97
								BVS Cl: 1.02	

Bond distances (Å) are underlined. Calculated bond valences relatively to S (/S:) or Cl (/Cl:) take into account the s.o.f. of S or Cl, respectively.

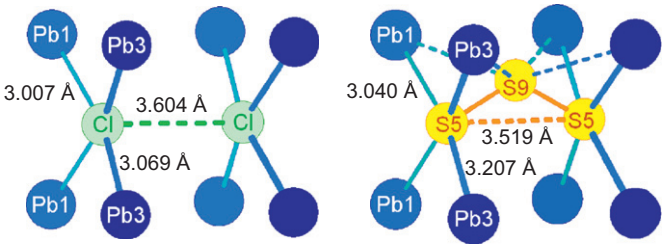

Fig. 2. Coordination of the Cl atom pair in $Pb_{3+x}Sb_{3-x}S_{7+x}Cl_{1+x}$ (left), compared to that of the S_3 trimer in $Pb_6Sb_6S_{14}(S_3)$ (right).

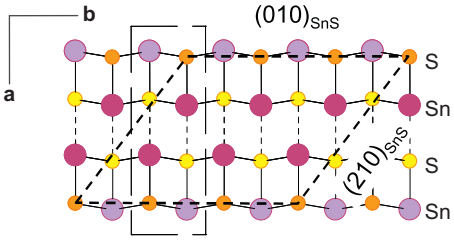

Fig. 3. Projection along c of the crystal structure of SnS. The lozenge (dashed line) indicates the archetypal $Sn_{12}S_{16}$ rod constituting the building block of $Pb_{3+x}Sb_{3-x}S_{7+x}Cl_{1+x}$. Dashed bonds separate two-atom-thick layers along a. Dark and light atoms have their z coordinate close to 0 and 0.5, respectively.

A close structural relationship also exists with the series $ALn_{1\pm x}Bi_{4\pm x}S_8$ (A = K, Rb; Ln = La, Ce, Pr, Nd) defined by Iordanidis et al. [46]. On the basis of the structure of $KLa_{1.28}Bi_{3.72}S_8$ (Fig. 5), one can see that the projections of this structure and of $Pb_{3+x}Sb_{3-x}S_{7-x}Cl_{1+x}$ along their short axis are very similar. Nevertheless, the coordinations of Sb and Bi inside the rods are different: Bi has a distorted octahedral environment, and the constitutive rod is related to the PbS archetype, and not to the SnS one, that gives a $b/2$ shift between the two internal opposite Bi_3S_4 ribbons; Sb has a distorted monocapped triangular prismatic environment (one hemi-octahedron + two longer bonds), with all Sb atoms within a rod at (or close to) $z = 0$.

Another topological difference is the geometry of the interconnection between four constitutive rods (ellipses in

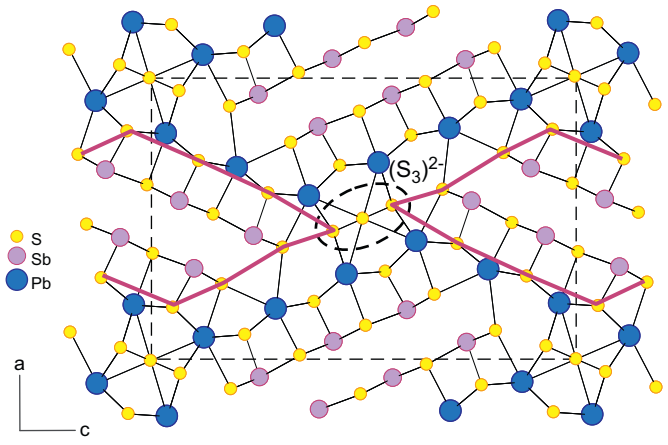

Fig. 4. Projection along b of the crystal structure of $Pb_6Sb_6S_{14}(S_3)$. The $(S_3)^{2-}$ trimer (within the dashed ellipse) connects two rods along c via their acute edges.

Figs. 1 and 5). This interconnection is shorter along c of $KLa_{1.28}Bi_{3.72}S_8$, due to the lying monocapped coordination of the two (Bi,La) prismatic sites along this direction, relatively to the corresponding interconnection along b of $Pb_{3+x}Sb_{3-x}S_{7+x}Cl_{1+x}$ (no bond between Pb1 and Cl atoms along this direction). According to Makovicky's classification [40], this rod interconnection gives a "rod-layer" of type 4 for "KLaBi", and of type 10 for $Pb_{3+x}Sb_{3-x}S_{7+x}Cl_{1+x}$. The compression along one direction ($c_{KLaBi} < b_{PbSb}$) is counterbalanced by an expansion along the other direction ($a_{KLaBi} > a_{PbSb}$). Thus the c/a ratio of "KLaBi", 1.296, is smaller than the b/a ratio of 1.521 for "PbSb", but the unit cell volumes are very close ($\delta V/V \sim 3\%$—Table 6). These topological differences explain the distinct space groups, *Pnma* for $KLa_{1.28}Bi_{3.72}S_8$ and *Pbam* for $Pb_{3+x}Sb_{3-x}S_{7-x}Cl_{1+x}$, corresponding here to a structural relationship distinct from a true homeotypy.

As pointed out by Iordanidis et al. [46], the compound "$Ce_{1.25}Bi_{3.78}S_8$" of Ceolin et al. [47] actually corresponds to the K/Ce/Bi sulfide of the series $ALn_{1\pm x}Bi_{4\pm x}S_8$, with probable composition $KCe_{1\pm x}Bi_{4\pm x}S_8$. It was presented by Makovicky [40] as a typical example of a "pure rod structure".

Table 6
Unit cell data of $Pb_{3+x}Sb_{3-x}S_{7+x}Cl_{1+x}$ and closely related chalcogenides

N	Compound	Sp. Gr.	Elong. axis (Å)	Second axis (Å)	Stacking axis (Å)	V (Å^3)	Z
2	$Pb_{3+x}Sb_{3-x}S_{7+x}Cl_{1+x}$[a]	*Pbam*	4.0591	15.194	23.035	1420.6	4
2	$Pb_6Sb_6S_{14}(S_3)$ [34]	$P2_12_12$	4.0400	15.328	23.054	1427.6	2
2	$Pb_6Sb_6Se_{14}(Se_3)$ [43]	*Pbam*	4.134	15.835	24.043	1573.9	2
2	$Sr_6Sb_6S_{14}(S_3)$ [42]	$P2_12_12_1$	8.2871	15.352	22.873	2910.0	4
2	$Eu_6Sb_6S_{14}(S_3)$ [44]	$P2_12_12_1$	8.236	15.237	22.724	2851.7	4
2	$KLa_{1.28}Bi_{3.72}S_8$ [46]	*Pnma*	4.0712	16.652	21.589	1463.63	4
2	$Ce_{1.25}Bi_{3.78}S_8$ [47]	*Pnma*	4.053	16.55	21.52	1443.50	4
~2	$Pb_{23}Sb_{25}S_{60}Cl$ [21]	$P1^-$	8.276	17.392	19.505	2727.2[b]	1

[a]This study.
[b]With $\alpha = 83.527°$, $\beta = 77.882°$, $\gamma = 89.125°$.

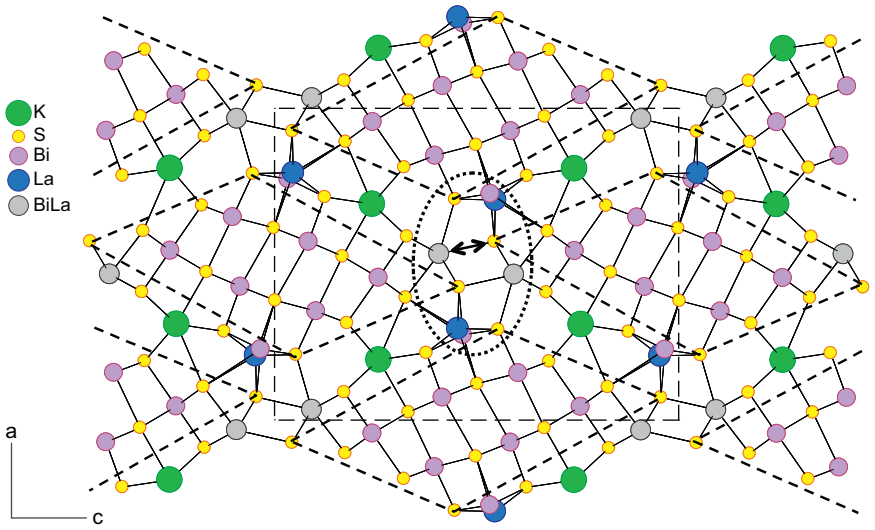

Fig. 5. Projection along b of the crystal structure of $KLa_{1.28}Bi_{3.72}S_8$. The doted ellipse surrounds the connection between four rods; two rods along c are connected via *Me*–S bonds (double arrow).

Dadsonite, $Pb_{23}Sb_{25}S_{60}Cl$, is also a very close structural derivative. Its crystal structure [21] is composed of two types of "rod-layers", with constitutive rods $R1$ and $R2$ (Fig. 6). $R1$ is built from the same kind of rods than in $Pb_{3+x}Sb_{3-x}S_{7-x}Cl_{1+x}$, but with two adjacent rods bridging together via two Sb–S bonds (rod-layer type 3, and type 10 for $Pb_{3+x}Sb_{3-x}S_{7-x}Cl_{1+x}$ [40]). In the second rod-layer (type 5 [40]), two adjacent rods $R2$ are joined together by merging the two Cl atoms from each primitive rod in a common, half-filled Cl position ("S1" position of Makovicky et al. [21]). Such a specific Cl position, alternating with a vacancy along a, was predicted to govern the ~8 Å periodicity [20]. Taking into account this ~8 Å periodicity, the first rod-layer has the composition $M_{24}S_{32}$, the second one, $M_{24}S_{28}Cl\square$ ($\square$: anion vacancy), giving the stoichiometric ideal formula $Pb_{23}Sb_{25}S_{60}Cl$. These two geometrical operations enhance the compression along c of the structure of dadsonite relatively to $Pb_{3+x}Sb_{3-x}S_{7-x}Cl_{1+x}$ (Table 6), as indicated by the elongation of the doted ellipse in Fig. 6. With $c = 17.33$ Å and $a\sin\beta = 18.93$ Å, one obtains $c/a = 0.915$ ($\delta V/V \sim -4\%$).

4. The problem of short-range ordering within the *M* sites

The absence of superstructure diffraction spots in the X-ray investigation of $Pb_{3+x}Sb_{3-x}S_{7+x}Cl_{1+x}$ indicates no long-range ordering along c of Pb and Sb positions within the M sites of the structure. This is related to any Pb and Sb s.o.f. values within these M sites. Nevertheless, taking into account the crystal structure of $Sr_6Sb_6S_{14}(S_3)$ [42] as well as those of some complex Pb–Sb or Pb–As sulfosalts, which present a superstructure ordering along their short axis, it is possible to explain the distribution of Pb and Sb in distinct M sub-sites as the consequence of short-range ordering due to the aggregation of Sb atoms in finite $(Sb,As)_nS_m$ polyanions (here chain fragments).

4.1. Aggregation of Sb atoms in the structure of $Sr_6Sb_6S_{14}(S_3)$

Fig. 7a is a representation of the crystal structure of $Sr_6Sb_6S_{14}(S_3)$ restricted to the half-central part of the constitutive ribbon, which is focused on the Sb atoms

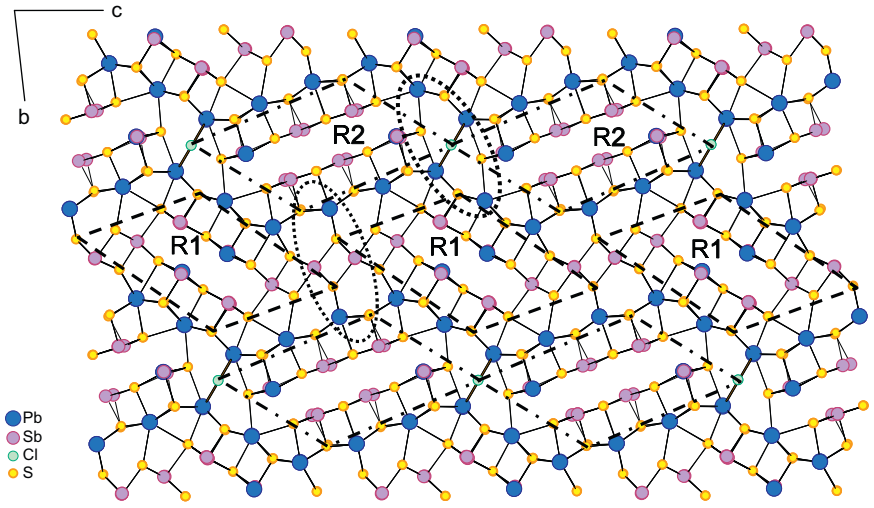

Fig. 6. Projection along *a* of the crystal structure of dadsonite, $Pb_{23}Sb_{25}S_{60}Cl$. The two rod types, *R*1 and *R*2, induce two types of connection between four rods (doted ellipses).

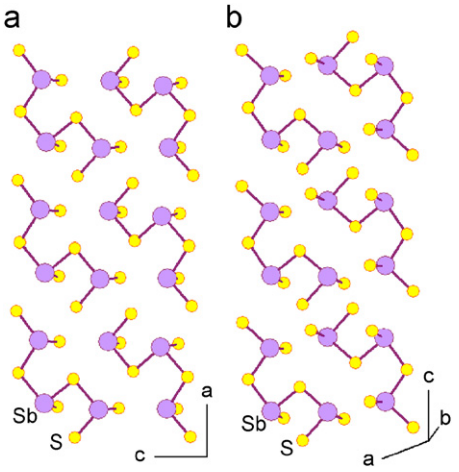

Fig. 7. Sb–S aggregation in $Sr_6Sb_6S_{14}(S_3)$ (a) and $TlSb_3S_5$ (b): formation of $[Sb_3S_7]^{5-}$ polyanions oblique to the elongation axis (*a* and *c*, respectively).

(Sb1–Sb6) and their strong bonded S atoms ($d_{(Sb-S)}<2.70$ Å). It shows clearly the aggregation of the Sb atoms to form with S atoms the polyanion $[Sb_3S_7]^{5-}$, in a crankshaft fashion oblique to the *a* elongation direction. This aggregation has also been emphasized by Jin et al. [44] for the isotype $Eu_6Sb_6S_{14}(S_3)$. Such a crankshaft organization is quite identical to that depicted initially by Makovicky and Balić-Žunić [48] in the structure of $TlSb_3S_5$ (Fig. 7b).

The aggregation of Sb or As atoms in triangular pyramidal coordination with S atoms to constitute finite $(Sb,As)_nS_m$ chains is known in various sulfosalts. Its role has been emphasized first in $PbAgSb_3S_6$ (senandorite [49]), with a $Sb_{14}S_{28}$ chain, then in Pb–As natural sulfosalts (sartorite, $Pb_8Tl_{1.5}As_{17.5}S_{35}$ [50]; rathite-dufrénoysite, $Pb_8Pb_{4-x}(Tl_2As_2)_x(Ag_2As_2)As_{16}S_{40}$ [51]) and recognized by these last authors in synthetic Ba derivatives of rathite, $Ba_{12}Sb_{18.64}S_{40}$ and $Ba_{10.48}Pb_{5.52}Sb_{16}S_{40}$ [42]. A recent example concerns the resolution of the crystal structure of the chloro-sulfosalt dadsonite, $Pb_{23}Sb_{25}S_{60}Cl$ [21].

In all these compounds, such an aggregation induces $a\sim 4n$ Å superstructure. Generally one has $n=2$ (“~8 Å superstructure”), but higher *n* values do exist: 4 or 6 in the andorite series $Pb_{3-2x}Ag_xSb_{2+x}S_6$ [49], or 9 for a sartorite variety [50]. It is worth noting that the degree of Sb aggregation is controlled by a steric constraint, i.e. the necessity to adjust the central net of Sb or As small polyhedra within a rod, to that of large polyhedra of the bigger countercation (Pb^{2+}, Sr^{2+}, Ba^{2+}, Eu^{2+}, Tl^{+}, K^{+}, trivalent light *Ln*) at the surface of the rod. As a general rule, an increase of the ionic radius or atomic ratio of this countercation goes against Sb aggregation, and will induce a decrease of the size of $(Sb,As)_nS_m$ chain fragments, down to isolated SbS_3 groups.

In Pb–Sb sulfosalts, another way to adjust Sb sub-domains to Pb sub-domains is obtained by some Pb substitution on Sb sites, eventually equilibrated by a reciprocal Sb substitution on Pb sites. This has been exemplified for $Pb_4Sb_6S_{13}$ and $Pb_5Sb_4S_{11}$ [52], and it appears here also as an important mechanism in lead chloro-sulfosalts, through the substitution $Sb+S\rightarrow Pb+Cl$, favored by an increasing temperature.

4.2. Sb aggregation and bond valence calculations

According to these examples, Sb (or As) aggregation governs the superstructure. When the coordination of As or Sb is enlarged to the five nearest S atoms, these atoms then present a dissymmetric pyramidal coordination with a trapezoidal basis [53]. If the true (super-)structure is not solved, but only the mean (sub-)structure, this gives a pseudo-rectangular coordination, and one observes a strong decrease of the bond valence sum (BVS_{Sb}) for trivalent Sb. For instance, Table 7 compares these sums for

Sb atoms in $Sr_6Sb_6S_{14}(S_3)$ according to three structural models:

- BVS_{Sb} obtained for the true (super-)structure (model I);
- BVS_{Sb} for the (sub-)structure, with mean S positions, but split Sb ones (model II—Fig. 8a);
- BVS_{Sb} for the (sub-)structure, with mean S and Sb positions (model III—Fig. 8b).

For the true structure, BVS_{Sb} is very good for all Sb positions, with a mean value of 2.96. For model II, only one BVS_{Sb} is tolerable (2.80); the other values are bad, down to 2.21, with a mean value equal to 2.53. For model III, all BVS_{Sb} are bad, with a mean value down to 2.38. The crystal (sub-)structure solution proposed for $Pb_{3+x}Sb_{3-x}S_{7-x}Cl_{1+x}$ corresponds to a model-II type. Table 8 gives the detail of bond valence calculations. For Sb sub-positions in *M* sites, BVS_{Sb} varies from 3.04 down to 2.17, with a mean value equal to 2.57.

These results show the inaccuracy of bond valence calculations for a sub-structure when the cation presents a strong dissymmetric coordination, here related to a high stereochemical activity of the lone electron pair of trivalent Sb. This aspect was previously underlined for complex Pb–Sb oxy- and chloro-sulfosalts, where the true ~8 Å structure does exist, but could not be resolved: $Pb_{14}Sb_{30}S_{54}O_5$ [54], $Pb_9Sb_{10}S_{23}ClO_{0.5}$ [25], $(Cu,Ag)_2Pb_{21}Sb_{23}S_{55}ClO$ [22].

Table 7
Bond valence sums for Sb positions in $Sr_6Sb_6S_{14}(S_3)$ according to the true 8 Å structure (model I), the 4 Å substructure with mean S positions (model II), and the 4 Å substructure with mean S and Sb positions (model III)

	Sb1	Sb2	Sb3	Sb4	Sb5	Sb6	Mean
Model I	3.08	2.90	2.95	2.92	2.86	3.07	2.96
Model II	2.37	2.50	2.60	2.21	2.80	2.69	2.53
	(Sb1 + Sb2)		(Sb3 + Sb4)		(Sb5 + Sb6)		
Model III	2.31	2.26	2.57	2.38			

4.3. The structural role of Pb in M sites

In the reduced (sub-)structure (model II) of $Sr_6Sb_6S_{14}(S_3)$, the Sb sub-positions (Fig. 8a) are shifted obliquely (“up” and “down” by symmetry) or sub-perpendicularly (“left” or “right”) to the elongation *a*-axis, relatively to the Sb mean positions of model III (Fig. 8b):

- Sb1 is shifted up, and Sb2 right, relatively to Sb(1 + 2) mean position;
- Sb3 and Sb4 are shifted right and left, respectively, relatively to Sb(3 + 4) mean position;
- Sb5 and Sb6 are shifted left and up relatively to Sb(5 + 6) mean position.

Thus there is no shift up for the central Sb positions, contrary to the solution proposed for $Pb_{3+x}Sb_{3-x}S_{7-x}Cl_{1+x}$ (Fig. 9). This is probably due to Pb incorporation within the *M* sites, as the presence of a Pb atom within one *M* site will necessarily break the regular organization of $[Sb_3S_7]^{5-}$ polyanions, and will favor the formation of other Sb_nS_m fragments.

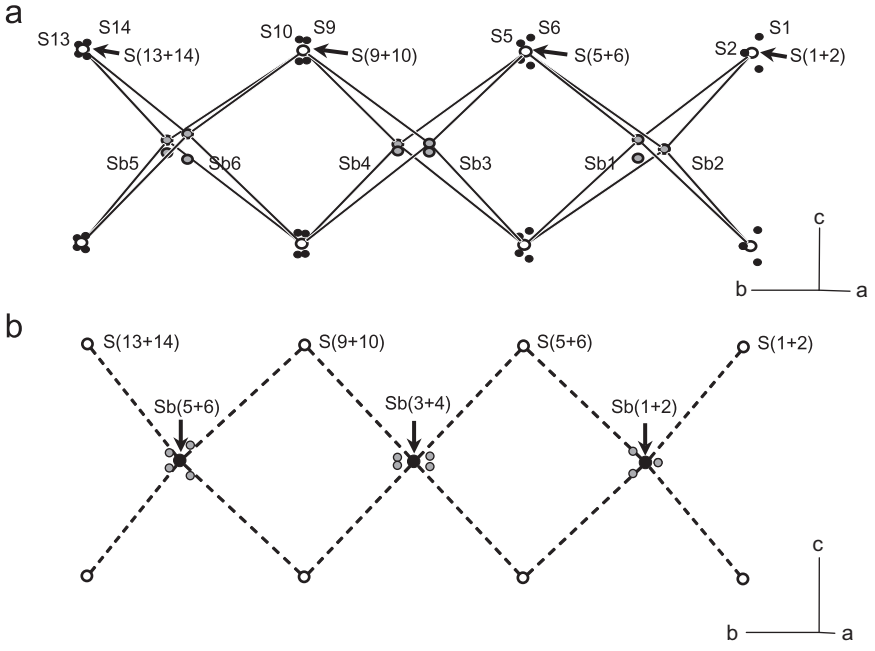

Fig. 8. Sb and S sub-positions in the substructure of $Sr_6Sb_6S_{14}(S_3)$: (a) mean S positions and split Sb positions (model II—for clarity, some Sb–S bonds have been omitted) and (b) mean S and Sb positions (model III).

Table 8
Bond valence sums (BVS) for Sb and Pb sub-positions within M sites of $Pb_{3+x}Sb_{3-x}S_{7+x}Cl_{1+x}$

Site	Atom	(S,Cl)1	(S,Cl)2	(S,Cl)3	S4	S5		S6	S7	BVS cation	Site ratio	BVS site[a]
*M*4	Pb4			2.890	2.734 × 2	3.082 × 2		3.397 × 2				2.75
				0.38	0.61 × 2	0.24 × 2		0.10 × 2		2.28	× 0.05	
	Sb4		2.416		2.562	2.800	3.123	3.671				
			1.10		0.74	0.39	0.16	0.04				
					2.912			3.924		2.74	× 0.85	
					0.29			0.02				
	Sb4A			2.430	2.508 × 2	3.224 × 2		3.822 × 2		3.04	× 0.10	
				1.06	0.85 × 2	0.12 × 2		0.02 × 2				
*M*5	Pb5		2.801			2.923 × 2	3.569 × 2	2.877 × 2				2.39
			0.48			0.36 × 2	0.06 × 2	0.41 × 2		2.14	× 0.10	
	Sb5		2.498			2.757	3.720	2.678				
			0.88			0.44	0.03	0.54		2.33	× 0.60	
						3.059	3.979	2.988				
						0.19	0.02	0.23				
	Sb5A		2.481			2.631 × 2	3.879 × 2	3.120 × 2				
			0.92			0.14 × 2	0.02 × 2	0.16 × 2		2.50	× 0.10	
	Sb5B		2.468			3.166 × 2	3.892 × 2	2.591 × 2				
			0.95			0.14 × 2	0.02 × 2	0.68 × 2		2.63	× 0.20	
*M*6	Pb6	2.625			3.574 × 2			3.129 × 2	2.727 × 2			2.46
		0.77			0.06 × 2			0.21 × 2	0.62 × 2	2.55	× 0.30	
	Sb6	2.478			3.743 × 2			3.286 × 2	2.576 × 2			
		0.93			0.03 × 2			0.10 × 2	0.71 × 2	2.61	× 0.40	
	Sb6B	2.554			3.451			2.818	2.525			
		0.75			0.07			0.37	0.82	2.17	× 0.30	
					3.862			3.308	3.064			
					0.02			0.10	0.19			

BVS for each M site is the total of BVS for cations within this site, according to their site ratio. Bond distances (Å) are underlined; below each are given corresponding bond valences.
[a]Theoretical BVS for *M*4: 2.95; for *M*5: 2.90; for *M*6: 2.70.

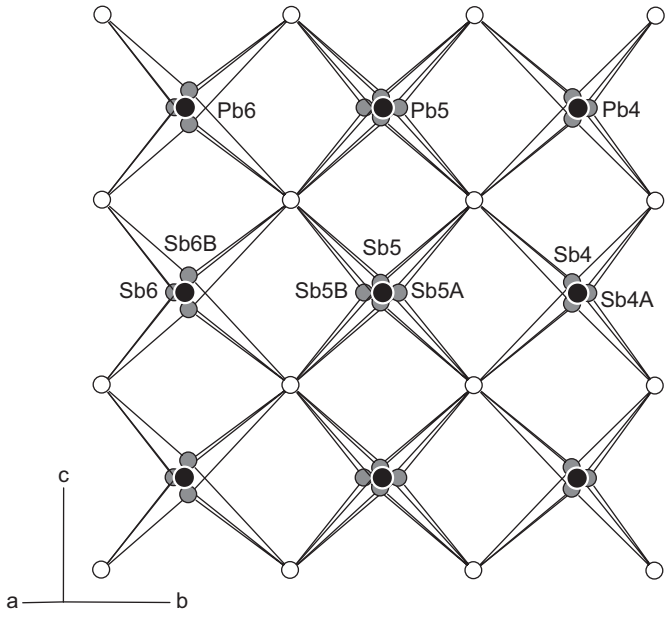

Fig. 9. Sb (gray) and Pb (black) sub-positions in M sites of $Pb_{3+x}Sb_{3-x}S_{7+x}Cl_{1+x}$.

This explanation is supported by the Sb aggregation described in the crystal structure of dadsonite, $Pb_{23}Sb_{25}S_{60}Cl$ [21], as the result of quite definite bonding schemes on the 8 Å level. In rod $R2$ (Fig. 10), where Pb substitutes for Sb in one of the two marginal sites, the Sb central position is shifted right or left relatively to its substructure mean position; but in rod $R1$, where Pb substitutes for Sb in the central position, this Sb atom is only shifted up.

In $Pb_{3+x}Sb_{3-x}S_{7-x}Cl_{1+x}$, Pb substitution over all the three M sites will induce *a fortriori* a more complex distribution of Sb sub-positions, with more irregularities in the aggregation of Sb atoms, and thus a long range disorder, precluding the apparition of any superstructure.

5. The homologous series $Pb_{(2+2N)}(Sb,Pb)_{(2+2N)}S_{(2+2N)}(S,Cl)_{(4+2N)}Cl_N$ and related structures

5.1. Definition of the homologous series

$Pb_{3+x}Sb_{3-x}S_{7-x}Cl_{1+x}$ and its homeotypes correspond to the $N = 2$ members of a homologous series (Table 9). The $N = 1$ primitive member is the lead–antimony chlorosulfide synthesized by Kostov-Kytin et al. [32], with composition $Pb_{4.32}Sb_{3.68}S_{8.68}Cl_{2.32}$, or $Pb_{4+x}Sb_{4-x}S_{9-x}Cl_{2+x}$ ($x = 0.32$). Its crystal structure is represented in Fig. 11a, where zigzag lines permit a cut-out of two types of

corrugated slabs A and B alternating along *b*. The B slab containing the Cl atoms in the middle is symmetric, with structural formula $Pb_2(Sb,Pb)_2S_2(S,Cl)_2Cl$; on the other hand, the A slab is dissymmetric, with formula $Pb_2(Sb,Pb)_2S_2(S,Cl)_4$. The stacking sequence is ABA′B′A…, with resulting formula $Pb_4(Sb,Pb)_4S_4(S,Cl)_6Cl$.

In Fig. 11b, the crystal structure of $Pb_{3+x}Sb_{3-x}S_{7-x}Cl_{1+x}$ has been cut out similarly in two topologically equivalent A and B slabs alternating in the *b* direction, but with the new sequence ABBABBA…. It thus appears as a higher, $N=2$ homolog of the primitive $N=1$ homolog $Pb_{4+x}Sb_{4-x}S_{9-x}Cl_{2+x}$, according to the general combination (A + *N*B) which defines the homologous series. Its structure formula is $Pb_6(Sb,Pb)_6S_6(S,Cl)_8Cl_2$, and the general formula for this homologous series, $Pb_{(2+2N)}(Sb,Pb)_{(2+2N)}S_{(2+2N)}(S,Cl)_{(4+2N)}Cl_N$. Pb-for-Sb and Cl-for-S substitutions in various ratios permit to fit the charge balance whatever the *N* value is.

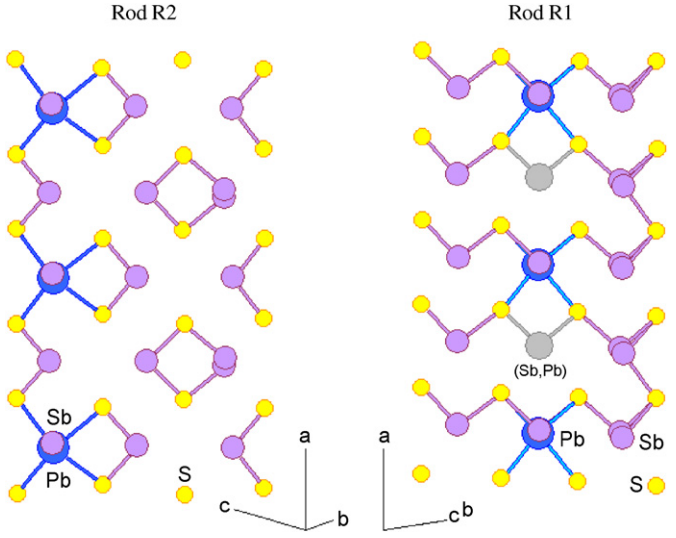

Fig. 10. Sb aggregation in dadsonite within *R*1 and *R*2 rods (according to [21], modified).

5.2. Chemical varieties of the $N=1$ homolog $Pb_{4+x}Sb_{4-x}S_{9-x}Cl_{2+x}$

The synthetic compound "$Pb_4Sb_4S_{11}$" [55] was considered by Kostov-Kytin et al. [32] as the Cl-free isotypic derivative of their phase $Pb_{4.32}Sb_{3.68}S_{8.68}Cl_{2.32}$, but the proposed crystal structure is debatable. First, its formula does not respect the charge balance: while there are two negative charges in excess, the structure does not present any S–S bonding or S vacancy which could neutralize this anion excess. Secondly, the bond valence sum calculated for the S1 atom substituting for Cl atom of Kostov-Kytin's phase is very low (1.20 valence unit for 4 Pb–S bonds of 2.994 Å), that would be in better accordance with a Cl atom, as the same calculation considering now 4 Pb–Cl bonds would give a total of 1.14 valence unit. Clearly, "$Pb_4Sb_4S_{11}$" is in fact a variety of the chloro-sulfosalt studied later by Kostov-Kytin et al. [32] (probably synthesized from an impure mixture).

The compound labeled "Phase Y' "(Table 1) of Moëlo [20] is another variety of this $N=1$ chloro-sulfosalt. It was obtained in a single run at 200 °C, from a mixture of PbS and Sb_2S_3 (molar ratio 5/4) in an aqueous solution saturated by $PbCl_2$ (duration: 3 weeks). On the basis of a total of 19 atoms, its electron probe microanalysis gave $Pb_{4.10(10)}Sb_{3.91(8)}S_{9.18(26)}Cl_{1.81(10)}$, close to the stoichiometric one proposed for the $N=1$ homolog, $Pb_4Sb_4S_9Cl_2$. Its published X-ray powder diagram (XRPD) appears similar, but not quite identical, to that calculated for the phase $Pb_{4+x}Sb_{4-x}S_{9-x}Cl_{2+x}$ of Kostov-Kytin et al. [32]; it is closer to the XRPD calculated for its isotype "$Pb_4Sb_4S_{11}$" [55]. The XRPD of Phase Y' has been indexed on this model, leading to the unit cell parameters (Table 9): $a=4.059(2)$, $b=14.877(5)$, $c=15.480(6)$ Å. The unit cell volume (934.7(11) Å^3) is significantly smaller than that of the phase of Kostov-Kytin et al. [32], in accordance with its lower Pb content.

In Table 9, the comparison of the unit cell parameters of $Pb_{4+x}Sb_{4-x}S_{9-x}Cl_{2+x}$ [32], "$Pb_4Sb_4S_{11}$" [55] and Phase Y' [20] shows intermediate values for "$Pb_4Sb_4S_{11}$", which

Table 9
Homologous derivatives of $Pb_{3+x}Sb_{3-x}S_{7+x}Cl_{1+x}$ and related polychalcogenides

N	Compound	Sp. gr.	Elong. axis (Å)	Second axis (Å)	Stacking axis (Å)	*V* (Å^3)	*Z*
1	$Pb_{4.32}Sb_{3.68}S_{8.68}Cl_{2.32}$ [32]	*Pbam*	4.09	15.04	15.51	954.1	2
1	$Pb_4Sb_4S_{11}$ [55]	*Pbam*	4.068	15.01	15.56	950	2
1	$Pb_{4.10}Sb_{3.91}S_{9.18}Cl_{1.81}$ [a,b]	*Pbam*	4.059	14.877	15.480	934.7	2
1	$K_2Pr_{2-x}Sb_{4+x}Se_8(Se_4)$ [56]	$Pna2_1$	4.1942	15.5534	33.881	2210.2	4
1	$BaBiSe_3$ [57]	$P2_12_12_1$	4.370	16.00	17.24	1205	8
1	$BaSbTe_3$ [57]	$P2_12_12_1$	4.635	16.94	18.09	1420	8
1	$BaBiTe_3$ [58]	$P2_12_12_1$	4.607	17.04	18.299	1436.5	8
1 + 2	$Pb_{10.38}Sb_{9.68}S_{23.08}Cl_{3.85}$ [20]	*P2/m*	4.06	15.19	19.42	1193.7	1
2	$Pb_{3+x}Sb_{3-x}S_{7+x}Cl_{1+x}$ [b]	*Pbam*	4.0600	15.196	23.119	1420.6	4
3	$SrBiSe_3$ [59]	$P2_12_12_1$	4.2610	15.7550	33.5520	2252.4	16

[a] Phase Y'.
[b] This study.

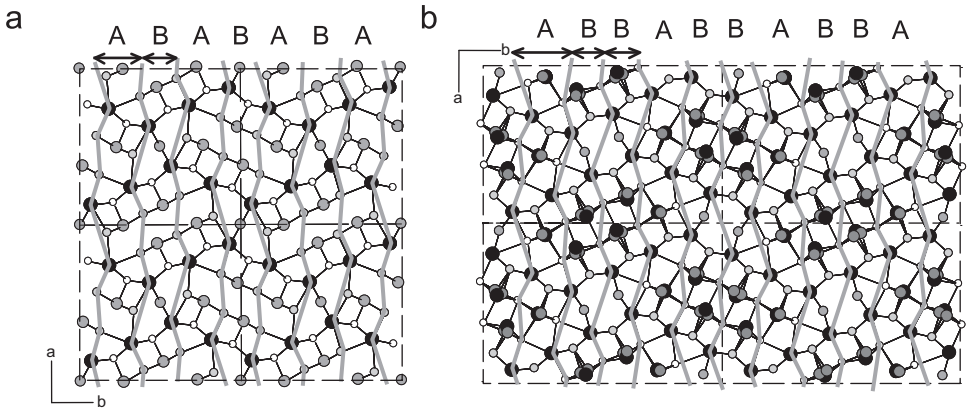

Fig. 11. Homologous relationship between the crystal structures of (a) $Pb_{4.32}Sb_{3.68}S_{8.68}Cl_{2.32}$ [28] and (b) $Pb_{3+x}Sb_{3-x}S_{7+x}Cl_{1+x}$ (this study). Two types of corrugated slabs (A and B, separated by gray broken lines) are stacked along b (double arrows).

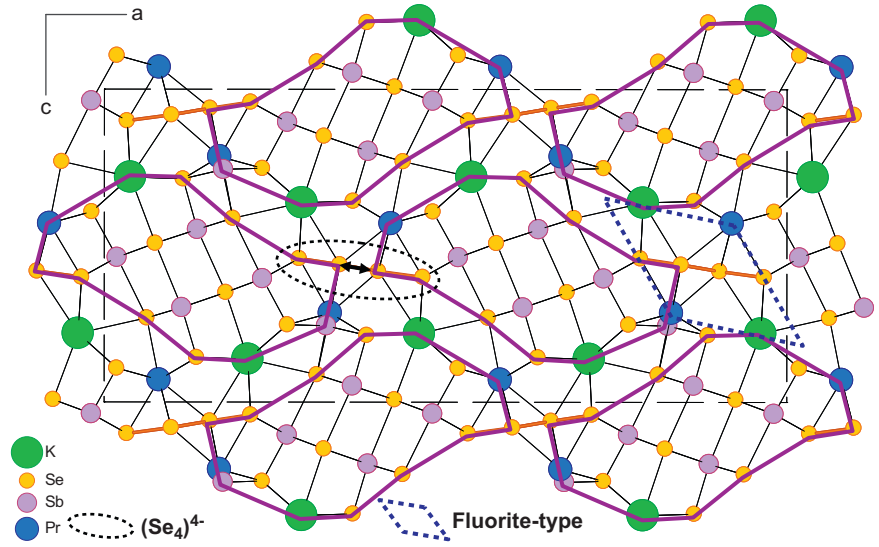

Fig. 12. Rod-based architecture of the crystal structure of $K_2Pr_{2-x}Sb_{4+x}Se_8(Se_4)$. Rod connection along a is controlled by $(Se_4)^{4-}$ aggregation (doted ellipse). The doted lozenge shows that the connection between four rods delimits a small rod of the fluorite type.

indicates that this phase has a higher Cl content relatively to Phase Y', with a x coefficient close to 0.25, on the basis of a linear interpolation between unit cell volumes.

Another synthetic Pb–Sb chloro-sulfosalt, labeled "Phase A" [27] (Table 1), presents a composition close to the $N=1$ homolog. It was obtained at 300 °C in a NH_4Cl–LiCl flux. On the basis of S + Cl = 11 atoms, its composition is $Pb_{4.31}Sb_{3.76}S_{8.83}Cl_{2.17}$ (x~0.2). Nevertheless, its XRPD is significantly different from those related to the $N=1$ homolog. A further crystallographic study by electron diffraction [30] indicated a monoclinic cell, with $a=21.97$, $b=21.3$, $c=8.05$ Å, $\beta=103°$ (with $c/2$ subcell). As the subcell volume is close to twice those of $N=1$ varieties, with a and b close to $\sqrt{2}b$ and $\sqrt{2}a$ of $Pb_{4.32}Sb_{3.68}S_{8.68}Cl_{2.32}$, respectively, the crystal structure of Phase A may be a monoclinic distortion of that of the $N=1$ homolog, favored by a low temperature, or the chemistry of the crystallization medium (for instance, NH_4^+ or Li^+ ions, which may enter the structure).

5.3. Polychalcogenide derivatives of this homologous series

As indicated above, $Pb_6Sb_6S_{14}(S_3)$ [34], $Sr_6Sb_6S_{14}(S_3)$ [42], $Pb_6Sb_6Se_{14}(Se_3)$ [43] and $Eu_6Sb_6S_{14}(S_3)$ [44] are polychalcogenide derivatives of the $N=2$ chloro-sulfosalt homolog.

As illustrated by Figs. 12 and 13, and Table 9, $K_2Pr_{2-x}Sb_{4+x}Se_8(Se_4)$ and its Ln isotypes (Ln = La, Ce, Pr or Gd [56]) correspond to the derived polyselenides of the homolog $N=1$, with the Cl position replaced by two Se, giving through polymerization with the two adjacent Se atoms a $[(Se_4)^{4-}]_\infty$ ribbon parallel to b (ellipse in Fig. 12). This Se ribbon forms with the four adjacent cations a rod of the fluorite type (blue-doted lozenge in Fig. 12). The rod-based description of Fig. 12 shows the rod interconnection along a through the $(Se_4)_\infty$ ribbon. According to Table 9, the ratio $(a/2)/c=1.089$ (1.031 for the $N=1$ chloro-sulfosalt). Fig. 13 represents the same structure according to the A- and B-slab stacking.

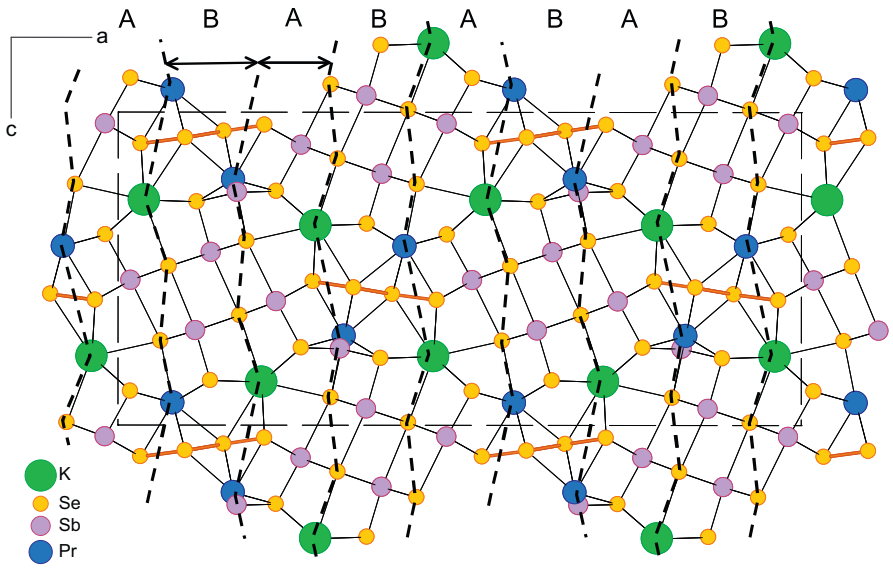

Fig. 13. Description of the crystal structure of $K_2Pr_{2-x}Sb_{4+x}Se_8(Se_4)$ as a $N=1$ homologous derivative of $Pb_{4.32}Sb_{3.68}S_{8.68}Cl_{2.32}$.

The synthetic compound $SrBiSe_3$ [59] was previously described as a higher homolog of $Pb_6Sb_6S_{14}(S_3)$ [34]. It appears as a close derivative of the $N=3$ homolog of the original structure of Kostov-Kytin et al. [32], as exemplified by Table 9 and Fig. 14. One has the new sequence ABBBABBBA…, but here, in the B slabs, the Cl atom is replaced by two Se atoms, and six neighboring Se atoms aggregate as two (Se_3) groups. The A and B slabs have the same composition $Sr_2Bi_2Se_6$, that gives for the unit sequence S3 (= A + 3B) the structural formula $Sr_8Bi_8Se_{24}$, or, more exactly, $Sr_8Bi_8Se_{18}(Se_3)_2$. For the hypothetic ideal $N=3$ homolog, the two (Se_3) groups ought to be replaced by 3 Cl atoms, that would oblige to replace one Bi by one Sr, to respect the charge balance: "$Sr_8(Bi_7Sr)Se_{18}Cl_3$".

The general formula of all these sub-homologous polychalchogenides is $M_{(2+2N)}(Pn)_{(2+2N)}Q_{(6+4N)}(Q_2)_N$ (M = a big cation, that is Pb, Sr, K or light *Ln*; *Pn*: pnictogen; *Q*: chalcogen), that is always a multiple of $MPnQ_3$: $(2+2N)$ $MPnQ_3$. With an increasing N value, the homolog structure will approach that of the *B* end-member. Such a BBB… stacking corresponds to the structure of $SrSbSe_2F$ [60]; Fig. 15 represents B slabs which cut obliquely the layered organization of $SrSbSe_2F$. Here the substitution of small fluorine atoms for bigger chalcogen atoms inside the fluorite-type layer precludes the formation of anion polymerization.

In all crystal structures considered up to now, their constitutive rods are always four-atom thick (see Fig. 3), with various widths. This thickness is determined by trivalent Sb or Bi present in the two inner atom layers. There are other close polychalcogenide derivatives, but with three-atom-thick rods, owing to tetravalent Sn: Sr_2SnSe_5 and $Sr_4Sn_2Se_9$ [61], Ba_2SnSe_5 [62] and monoclinic dimorph of Ba_2SnTe_5 [63]. Fig. 16 represents Sr_2SnSe_5, where the rod-layer connection is done by a $(Se3)^{2-}$ trimer. Sn is in the central atom layer, and adopt tetrahedral and octahedral coordinations.

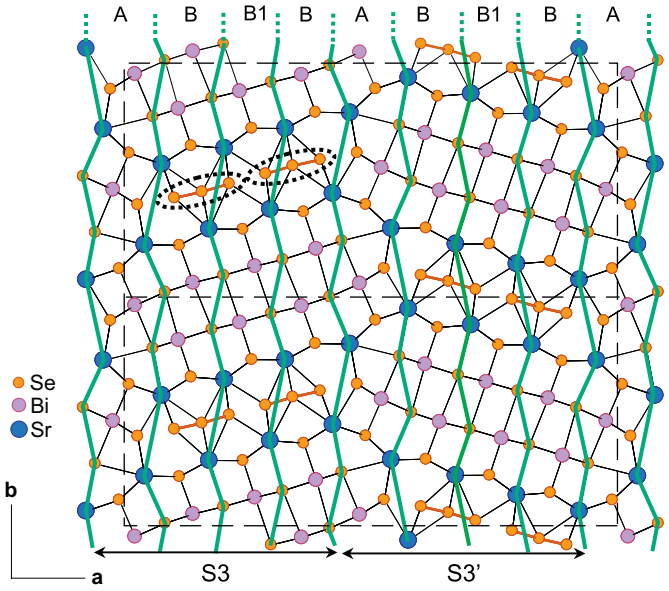

Fig. 14. Modular description of the crystal structure of $SrBiSe_3$ [59] as a $N=3$ homologous derivative of $Pb_{4.32}Sb_{3.68}S_{8.68}Cl_{2.32}$ archetype. Two (Se_3) groups overlap three B-type slabs. B1 slab slightly differs from B ones (no internal Se–Se bonding).

6. Application of the modular approach: prediction of the crystal structure of synthetic ~$Pb_{10}Sb_{10}S_{23}Cl_4$

"Phase Y" (Table 1 [20]), with proposed formula $Pb_{11}Sb_{10}S_{24}Cl_4$, was easily synthesized together with Pb–Sb sulfosalts at 200 °C from the reaction of a mixture of PbS and Sb_2S_3 with aqueous solutions enriched with dissolved $PbCl_2$ ($>2\times10^{-2}$ M). Its X-ray crystal study (XRPD and Weissenberg photographs) permitted to define the unit cell as monoclinic, space group *P*2, *Pm* or *P*2/*m*, with $a=19.42$, $b=4.06$, $c=15.19$ Å, $\beta=94.67°$. It thus appears that *b* and *c* parameters are very close to the two basic parameters of the homologous series defined above

(Table 9), while the third parameter is intermediate between those of the $N=1$ and 2 homologs. These relationships permitted to envisage Phase Y as the combined homolog $N=(1+2)$, resulting from the regular alternation of one $N=1$ layer with an $N=2$ one (Fig. 17). Such an alternation induces logically a monoclinic symmetry, and a rapid "paper + scissors" approach confirmed this hypothesis, with $b\sim19.8$ Å, and a β angle close to 95°.

As a second step, the predicted unit-cell atom structure of Phase Y (Fig. 17c) was constructed by pasting together an S1 slab of the $N=1$ homolog (Fig. 17a) with an S2' slab of the $N=2$ homolog (Fig. 17b) on the basis of a triclinic $P1$ space group, after geometric normalization of their parent unit cells (same two basic parameters than for Phase Y, without change of their respective unit cell volume). All sites were considered as pure sites, without Pb/Sb or S/Cl mixing. The comparison of the calculated XRPD (Diamond software [64]) with that published for Phase Y fully confirmed the general validity of the structural model (Fig. 18). This structure was finally fixed to its true space group $P2/m$, which was one among the three initially proposed for Phase Y [20]. Table 10 gives atom positions for this structure model; bond valence totals calculated for the five Pb positions vary from 1.98 up to 2.13. Unfortunately, a new XRPD performed on the original product of Moëlo [20] showed broad diffraction peaks indicating an alteration of the sample, that did not permit a refinement of the crystal structure on the basis of this model.

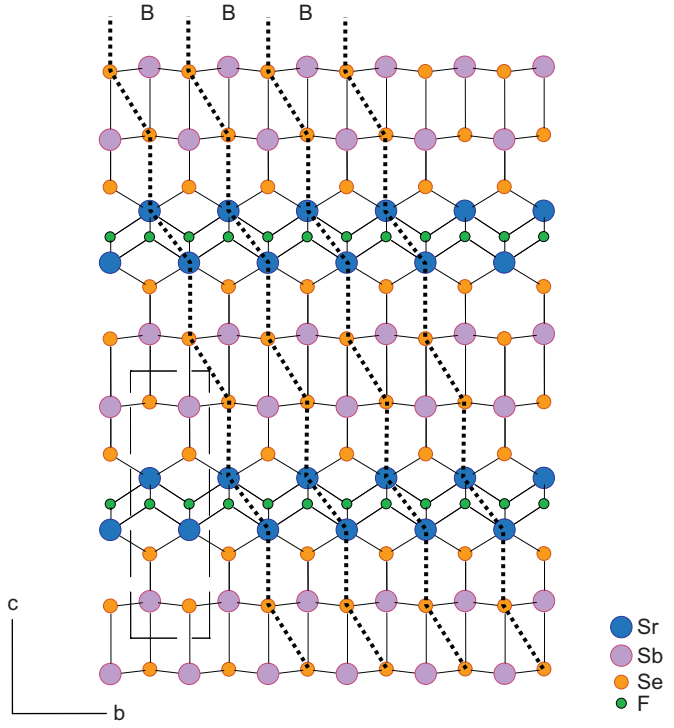

Fig. 15. Layered crystal structure of $SrSbSe_2F$ [60], with representation of oblique B-type slabs.

Involving pure atom positions, the structural formula of the predicted structure would be "$Pb_{10}Sb_{10}S_{24}Cl_3$", with $Z=1$, by combination of primitive "pure" formula "$Pb_4Sb_4S_{10}Cl$" ($N=1$) and "$Pb_6Sb_6S_{14}Cl_2$" ($N=2$). But "$Pb_4Sb_4S_{10}Cl$" does not respect the charge balance; to respect the Pb/Sb ratio, the stoichiometric formula ought to be "$Pb_4Sb_4S_9Cl_2$", giving finally $Pb_{10}Sb_{10}S_{23}Cl_4$ for the $N=(1+2)$ homolog. On the basis of the original electron microprobe analysis of Phase Y [20], with a total of 47 atoms, one obtains the formula $Pb_{10.38(22)}Sb_{9.68(17)}S_{23.08(52)}Cl_{3.85(22)}$, which is very close to the ideal formula $Pb_{10}Sb_{10}S_{23}Cl_4$ (and close to the formula proposed initially, i.e. $Pb_{11}Sb_{10}S_{24}Cl_4$). Such a formula, although stoichiometric, corresponds to 3 pure Cl positions, and an additional one distributed among some S positions.

The twinning described initially [20] is easily explained by a local stacking disorder of the two types of slabs A and B along c (for instance, two successive A (or B) slabs). With such a defect, the (001) stacking plane will act as a mirror (twinning operator).

7. Conclusion

The structural homeotypy evidenced between the new chloro-sulfide $Pb_{3+x}Sb_{3-x}S_{7-x}Cl_{1+x}$ and the polysulfide $Pb_6Sb_6S_{14}(S_3)$ has permitted to enlarge the homologous

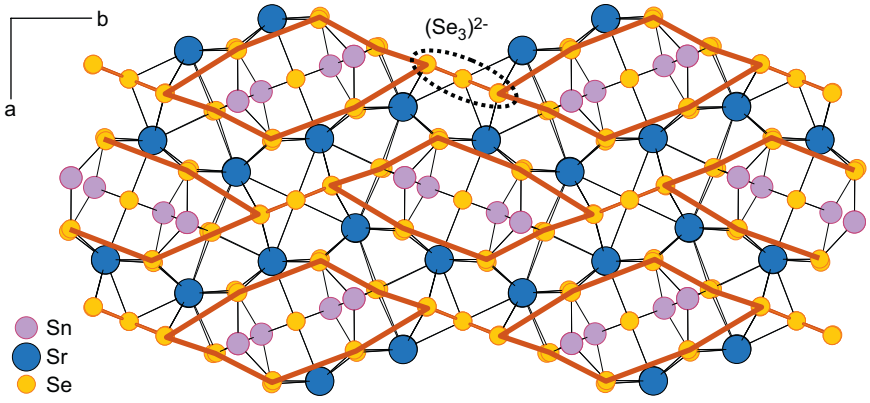

Fig. 16. Rod-based architecture of the crystal structure of Sr_2SnSe_5. The $(Se_3)^{2-}$ trimer (within the dashed ellipse) connects two rods along b (see Fig. 4 for comparison).

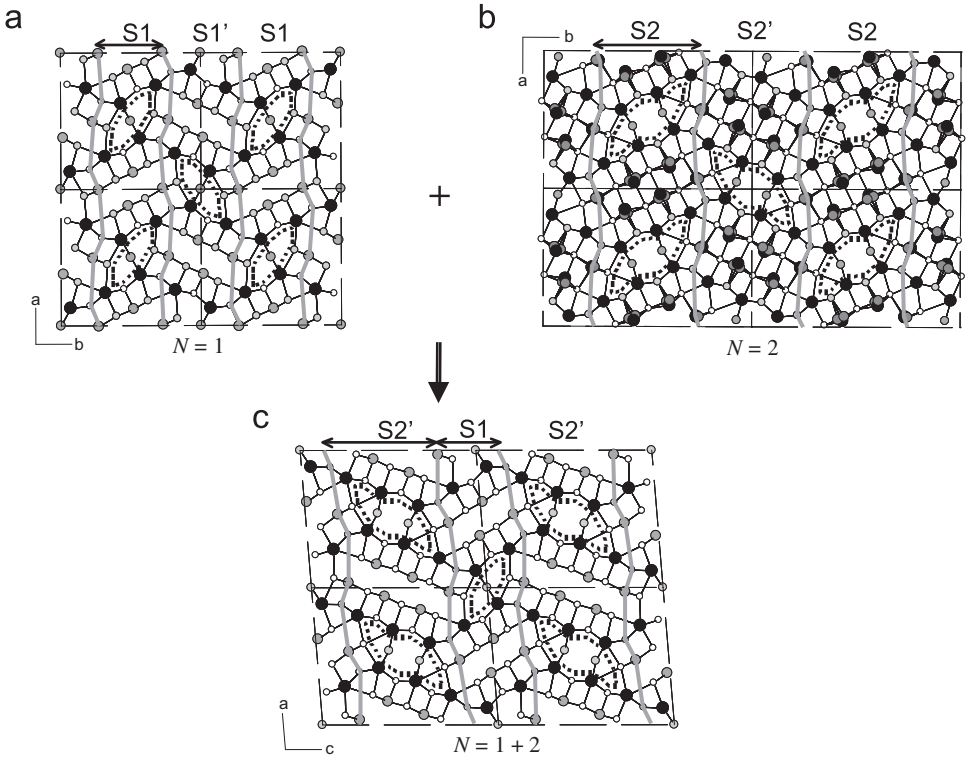

Fig. 17. Interpretation of the crystal structure of Phase Y (c), ~$Pb_{10}Sb_{10}S_{23}Cl_4$, as the $N = (1+2)$ homologous derivative of (a) $Pb_{4.32}Sb_{3.68}S_{8.68}Cl_{2.32}$ ($N = 1$) and (b) $Pb_{3+x}Sb_{3-x}S_{7+x}Cl_{1+x}$ ($N = 2$), by combination of their S1 and S2 constitutive slabs.

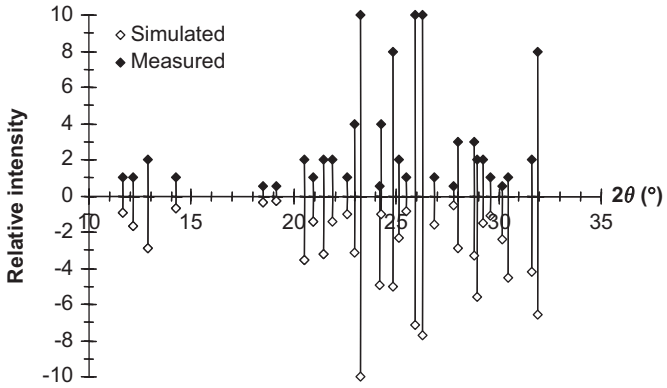

Fig. 18. Comparison of measured and simulated X-ray powder diagrams of Phase Y, ~$Pb_{10}Sb_{10}S_{23}Cl_4$.

Table 10
Structural model for Phase Y, ~$Pb_{10}Sb_{10}S_{23}Cl_4$: predicted atom coordinates

Atom	x	y	z	Atom	x	y	z
Pb1	0.879	0	0.055	S2	0.694	0	0.097
Pb2	0.278	0	0.146	S3	0.441	0	0.084
Pb3	0.795	0	0.251	S4	0.385	0.5	0.234
Pb4	0.690	0	0.445	S5	0.237	0.5	0.040
Pb5	0.413	0	0.347	S6	0.067	0	0.135
Sb1	0.624	0.5	0.015	S7	0.386	0.5	0.235
Sb2	0.533	0.5	0.185	S8	0.968	0	0.320
Sb3	0.036	0.5	0.215	S9	0.777	0.5	0.359
Sb4	0.935	0.5	0.414	S10	0.874	0	0.507
Sb5	0.170	0.5	0.383	S11	0.588	0	0.272
Cl1	0	0.5	0	S12	0.319	0.5	0.439
Cl2	0.541	0.5	0.413	S13	0.215	0	0.302
S1	0.877	0.5	0.165				

relationship defined by comparison of $Pb_6Sb_6S_{14}(S_3)$ with $SrBiSe_3$ [34]. Now the homologous series and its close derivatives includes about 15 compounds (Tables 6 and 9) corresponding to four homolog types ($N = 1$, $(1+2)$, 2 and 3). This constitutes a new example of the efficiency of the comparative modular approach to reveal the kinship between complex crystal structures.

This approach allowed to find a structure model for an ill-defined chloro-sulfosalt (Phase Y). More generally, such a definition of a new homologous series is a basis for the prediction of new homolog types; for instance, the $N = 3$ Pb–Sb chloro-sulfosalt would have the ideal structural formula $Pb_9Sb_7S_{18}Cl_3$. It is also a starting point for the synthesis of new chemical derivatives from known homologs. As an example, up to now there are no data about Pb–Sb chloroselenides, or Pb–Bi chloro-sulfides.

Appendix A. Supplementary material

Further details of the crystal structure investigation of $Pb_{3.45}Sb_{2.55}S_{6.55}Cl_{1.45}$ may be obtained from Fachinformationszentrum Karlsruhe, 76344 Eggenstein-Leopoldshafen, Germany (fax: (+49)7247 808 666; e-mail: crysdata@fiz-karlsruhe.de,

http://www.fiz-karlsruhe.de/crystal_structure_dep.html) on quoting the appropriate CSD number 418767.

References

[1] C. Doussier, P. Léone, Y. Moëlo, Solid State Sci. 6 (2004) 1387–1391.
[2] C. Doussier, G. André, P. Léone, E. Janod, Y. Moëlo, J. Solid State Chem. 179 (2006) 486–491.
[3] M.F. Bräu, F. Rau, A. Pfitzner, Z. Anorg. Allg. Chem. 632 (2006) 2119.
[4] J. Lewis, V. Kupcik, Acta Crystallogr. B 30 (1974) 848–852.
[5] T. Nilges, A. Pfitzner, Z. Kristallogr. 220 (2005) 281–294.
[6] M. Ruck, P.F. Poudeu Poudeu, T. Soehnel, Z. Anorg. Allg. Chem. 630 (2004) 63–67.
[7] P.F. Poudeu Poudeu, T. Soehnel, M. Ruck, Z. Anorg. Allg. Chem. 630 (2004) 1276–1285.
[8] M. Ruck, Z. Anorg. Allg. Chem. 628 (2002) 453–457.
[9] M. Ruck, Z. Anorg. Allg. Chem. 628 (2002) 1537–1540.
[10] P.F. Poudeu Poudeu, M. Ruck, J. Solid State Chem. 179 (2006) 3636–3644.
[11] L. Wang, Y.C. Hung, S.J. Hwu, H.J. Koo, M.H. Whangbo, Chem. Mater. 18 (2006) 1219–1225.
[12] J. Beck, S. Hedderich, K. Köllisch, Inorg. Chem. 39 (2000) 5847–5850.
[13] H. Nowottnick, K. Stumpf, R. Blachnik, H. Reuter, Z. Anorg. Allg. Chem. 625 (1999) 693–697.
[14] J. Beck, S. Schlüter, Z. Anorg. Allg. Chem. 631 (2005) 569–574.
[15] J. Beck, S. Schlüter, N. Zotov, Z. Anorg. Allg. Chem. 630 (2004) 2512–2519.
[16] J. Beck, S. Schlüter, M. Dolg, Angew. Chem. 40 (2001) 2287–2290.
[17] V. Krämer, Mater. Res. Bull. 11 (1976) 183–188.
[18] A. Garavelli, N.N. Mozgova, P. Orlandi, E. Bonaccorsi, D. Pinto, Y. Moëlo, Y.S. Borodaev, Can. Mineral. 43 (2005) 703–711.
[19] D. Pinto, E. Bonaccorsi, T. Balić-Žunić, E. Makovicky, Am. Mineral. (2008), in press.
[20] Y. Moëlo, Can. Mineral. 17 (1979) 595–600.
[21] E. Makovicky, D. Topa, W.G. Mumme, Can. Mineral. 44 (2006) 1499–1512.
[22] P. Palvadeau, A. Meerschaut, P. Orlandi, Y. Moëlo, Eur. J. Mineral. 16 (2004) 845–855.
[23] J.L. Jambor, Can. Mineral. 9 (1967) 191–213.
[24] Y. Moëlo, Thèse Doc. d'Etat no 82-01, Université de Paris VI-Document BRGM no. 57, Orléans, 1983.
[25] A. Meerschaut, P. Palvadeau, Y. Moëlo, P. Orlandi, Eur. J. Mineral. 13 (2001) 779–790.
[26] Y. Moëlo, O. Balitskaya, N. Mozgova, A. Sivtsov, Eur. J. Mineral. 1 (1989) 381–390.
[27] N.S. Bortnikov, N.N. Mozgova, A.I. Tsepin, V.V. Breskovska, Dokl. Akad. Nauk SSSR 244 (1979) 955–958.
[28] V.V. Kostov, J. Macíček, Eur. J. Mineral. 7 (1995) 1007–1018.
[29] C. Doussier, Y. Moëlo, P. Léone, A. Meerschaut, J. Solid State Chem. 180 (2007) 2323–2334.
[30] V.V. Breskovska, N.N. Mozgova, N.S. Bortnikov, A.I. Gorshkov, A.I. Tsepin, Mineral. Mag. 46 (1982) 357–361.
[31] E.A. Burke, C. Kieft, M.A. Zakrzewski, Can. Mineral. 19 (1981) 419–422.
[32] V.V. Kostov-Kytin, R. Petrova, J. Macíček, Eur. J. Mineral. 9 (1997) 1191–1197.
[33] G.V. Gigiadze, B.D. Guniaba, N.N. Mozgova, A.I. Tsepin, Y.S. Borodaev, Dokl. Akad. Nauk SSSR 277 (1984) 1464–1467.
[34] P. Orlandi, A. Meerschaut, P. Palvadeau, S. Merlino, Eur. J. Mineral. 14 (2002) 599–606.
[35] A.J.M. Duisenberg, J. Appl. Crystallogr. 25 (1992) 92–96.
[36] A.J.M. Duisenberg, L.M.J. Kroon-Batenburg, A.M.M. Schreurs, J. Appl. Crystallogr. 36 (2003) 220–229.
[37] G.M. Sheldrick, SHELXTL Version 5, Siemens Analytical X-ray Instruments Inc., 1994.
[38] N.E. Brese, M. O'Keeffe, Acta Crystallogr. B 47 (1991) 192–197.
[39] E. Makovicky, Fortschr. Mineral. 63 (1985) 45–89.
[40] E. Makovicky, Eur. J. Mineral. 5 (1993) 545–591.
[41] S. Del Bucchia, J.C. Jumas, M. Maurin, Acta Crystallogr. B 37 (1981) 1903–1905.
[42] K.S. Choi, M.G. Kanatzidis, Inorg. Chem. 39 (2000) 5655–5662.
[43] M. Ermidag-Kanes, J.W. Kolis, Z. Anorg. Allg. Chem. 628 (2002) 10–11.
[44] G. Jin, D.M. Wells, S.J. Crerar, T.C. Shehee, A. Mar, T.E. Albrecht-Schmidt, Acta Crystallogr. E 61 (2005) i116–i119.
[45] G.L. Schimek, J.W. Kolis, Inorg. Chem. 36 (1997) 1689–1693.
[46] L. Iordanidis, J.L. Schindler, C.R. Kannewurf, M.G. Kanatzidis, J. Solid State Chem. 143 (1999) 151–162.
[47] R. Ceolin, P. Toffoli, P. Khodadad, N. Rodier, Acta Crystallogr. B 33 (1977) 2804–2806.
[48] E. Makovicky, T. Balić-Žunić, Neues Jahrb Mineral. Abh. 165 (1993) 331–344.
[49] H. Sawada, I. Kawada, E. Hellner, M. Tokonami, Z. Kristallogr. 180 (1987) 141–150.
[50] P. Berlepsch, T. Armbruster, E. Makovicky, D. Topa, Am. Mineral. 88 (2003) 450–461.
[51] P. Berlepsch, T. Armbruster, D. Topa, Z. Kristallogr. 217 (2002) 581–590.
[52] E. Makovicky, T. Balić-Žunić, L. Karanovic, D. Poleti, J. Pršek, N. Jb. Miner. Mh. 2 (2004) 49–67.
[53] E. Makovicky, W.G. Mumme, N. Jb. Miner. Abh. 147 (1983) 58–79.
[54] Y. Moëlo, A. Meerschaut, P. Orlandi, P. Palvadeau, Eur. J. Mineral. 12 (2000) 835–846.
[55] I.V. Petrova, N.S. Bortnikov, E.A. Pobedimskaya, N.V. Belov, Dokl. Akad. Nauk SSSR 244 (1979) 607–609.
[56] J.H. Chen, P.K. Dorhout, J. Alloys Compd. 249 (1997) 199–205.
[57] K. Volk, G. Cordier, R. Cook, H. Schäfer, Z. Naturforsch. 35B (1980) 136–140.
[58] D.Y. Chung, S. Jobic, T. Hogan, C.R. Kannewurf, R. Brec, J. Rouxel, M.G. Kanatzidis, J. Am. Chem. Soc. 119 (1997) 2505–2515.
[59] R. Cook, H. Schäfer, Rev. Chim. Minér. 19 (1982) 19–27.
[60] H. Kabbour, L. Cario, Inorg. Chem. 45 (2006) 2713–2717.
[61] R. Pocha, D. Johrendt, Inorg. Chem. 43 (2004) 6830–6837.
[62] A. Assoud, N. Soheilnia, H. Kleinke, J. Solid State Chem. 178 (2005) 1087–1093.
[63] A. Assoud, S. Derakhshan, N. Soheilnia, H. Kleinke, Chem. Mater. (2004) 4193–4198.
[64] K. Brandenburg, H. Putz, Diamond 3a1 Version, Crystal Impact, Bonn, Germany, 2005.